JPE 16-5-5

http://dx.doi.org/10.6113/JPE.2016.16.5.1669
ISSN(Print): 1598-2092 / ISSN(Online): 2093-4718

A New Family of Non-Isolated Zero-Current Transition PWM Converters

Mohammad Rouhollah Yazdani[†], Mohammad Pahlavan Dust[*], and Poorya Hemmati[*]

[†,*]Department of Electrical Engineering, Isfahan (Khorasgan) Branch, Islamic Azad University, Isfahan, Iran

Abstract

A new auxiliary circuit for boost, buck, buck-boost, Cuk, SEPIC, and zeta converters is introduced to provide soft switching for pulse-width modulation converters. In the aforementioned family of DC–DC converters, the main and auxiliary switches turn on under zero current transition (ZCT) and turn off with zero voltage and current transition (ZVZCT). All diodes commutate under soft switching conditions. On the basis of the proposed converter family, the boost topology is analyzed, and its operating modes are presented. The validity of the theoretical analysis is justified by the experimental results of a 100W, 100 kHz prototype. The conducted electromagnetic emissions of the proposed boost converter are measured and found to be lower than those of another ZCT boost converter.

Key words: DC–DC converter, EMI, Soft switching, Zero current transition (ZCT), Zero voltage transition (ZVT)

I. INTRODUCTION

DC–DC pulse-width modulation (PWM) power converters are widely used in electrical and electronic systems, including renewable energy systems. Switching frequency is often increased to reduce the size and weight of power converters while increasing the power density. However, higher switching frequency leads to more switching losses and electromagnetic emissions. Soft switching techniques are indispensable to overcoming these issues [1]–[7].

Zero-current-transition (ZCT) methods are desirable approach in high power applications [8]–[14], particularly when IGBTs are used as the main switch. As the current becomes zero before the turning off of the switch, the IGBT current tailing losses are alleviated [15]. The ZCT converter proposed in [8] exerts no additional current stress on switches, but the turn-on of the main and auxiliary switches is hard switching, which decreases the efficiency. In [9], ZCS condition is provided for the switches by means of a high frequency resonant network; however, the capacitive losses of the MOSFET output capacitor at turn-on led to additional losses. An improved ZCT converter was introduced in [10] with reduced conduction losses, but the voltage stress of main diode is twice the output voltage. A comparative study on ZCT converters was presented in [11], and an improved ZCT boost converter was introduced; this converter transfers circulating energy to the output via a transformer, thereby increasing efficiency. However, this improved converter comprises more components than other ZCT converters. In [16], three coupled inductors were employed in a ZCS power factor correction boost converter to limit the reverse-recovery current of the output diode. However, five extra diodes are used in the snubber circuit, which increase the cost and the weight.

In [4], coupled inductors were employed to achieve a high voltage gain; however, the main and auxiliary switches operate under hard switching conditions, leading to higher switching losses and lower efficiency. A step-up converter proposed in [17] utilizes a snubber circuit comprising coupled inductors; this structure results in a ripple-free output current, but both switches are turned off under hard switching conditions.

In addition to efficiency, soft-switching conditions, and switch stresses, the electromagnetic interference (EMI) caused by power converters should be considered [18]–[21]. Several ZCT converters, such as those proposed in [12] and [13], exhibit high di/dt due to the reverse recovery of the main diode, which could generate more conducted

Manuscript received Feb. 8, 2016; accepted May 14, 2016
Recommended for publication by Associate Editor Chun-An Cheng.
[†]Corresponding Author: mro.yazdani@gmail.com
Tel: +98-31-35354001, Fax: +98-31-35354060, Isfahan (Khorasgan) Branch, Islamic Azad University
[*]Department of Electrical Engineering, Isfahan (Khorasgan) Branch, Islamic Azad University, Iran

electromagnetic emissions.

In the present work, a new family of ZCT PWM converters that use coupled inductors is introduced. In the proposed converters, the main and auxiliary switches turn on with ZCT and turn off with both ZCT and ZVT. Moreover, all diodes operate with soft switching condition, and the voltage stress of the main diode is less than twice the output voltage.

Providing ZCS condition at turn-off instant for both switches alleviates the tailing current loss of the IGBT. Furthermore, the lower conduction loss and cost of the IGBT with respect to MOSFET at high voltages makes the proposed auxiliary circuit suitable for high power applications. As the proposed converters have both ZCS and ZVS features, switching losses are almost zero, and they can operate at a higher switching frequency in comparison with their hard switching counterparts.

Utilizing coupled inductors in the proposed converters offers some advantages, such as providing ZVS condition for the main switch and diodes and lowering the current stresses of the switches. In the proposed family, the circulating energy of the auxiliary circuit is transferred to the output by the coupled inductors, thereby increasing overall efficiency. Note that the leakage inductance of the coupled inductors is absorbed by the resonant network and provides ZCS condition for the main switch at the turn-off instant.

The proposed ZCT converters have almost continuous and non-pulsating current waveforms. Moreover, the ZCT condition at turn-on and ZCT–ZVT at turn-off instant result in lower di/dt and dv/dt. Accordingly, the proposed family could potentially improve electromagnetic compatibility (EMC) [20]. Therefore, in addition to the efficiency and soft-switching issues, conducted EMI is evaluated in this work.

This paper is organized as follows. From the proposed converter family, the analysis of the boost topology and its theoretical waveforms are presented in Section II. The design procedure of the proposed converter is described in Section III. The experimental results of the converter prototype that confirm the theoretical analysis are presented in Section IV. The conducted electromagnetic emissions of the proposed converter are measured and compared with those of a similar ZCT boost converter in Section V. The topology variation of the proposed converter is detailed in Section VI, and the concluding remarks are given in Section VII.

II. CIRCUIT DESCRIPTION AND OPERATION

The circuit configuration of the proposed ZCT boost converter is shown in Fig. 1. The circuit components include the main inductor L_{in}, coupled inductors L_1 and L_2, output capacitor C_O, resonance capacitor C_r, main switch S_1, auxiliary switch S_a and its body diode D_1, and two other diodes, D_O and D_2. The total leakage inductance of the coupled inductors is shown by L_{lk}. To simplify the analysis, L_{in} and C_O are assumed to be sufficiently large to be modeled as a constant current and voltage source I_{in} and V_O, respectively. The turn ratio of the coupled inductors is $N_2/N_1=n$, i.e., $L_2=n^2L_1$. The proposed converter has eight operation intervals, as shown in Fig. 2.

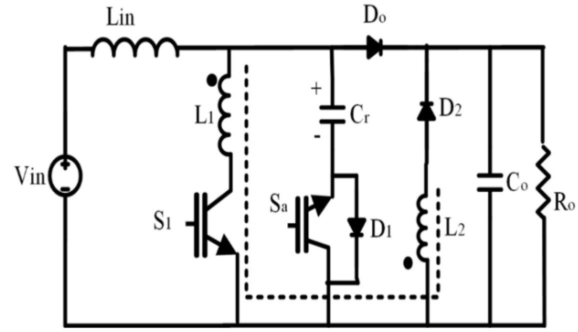

Fig. 1. Proposed ZCT PWM boost converter.

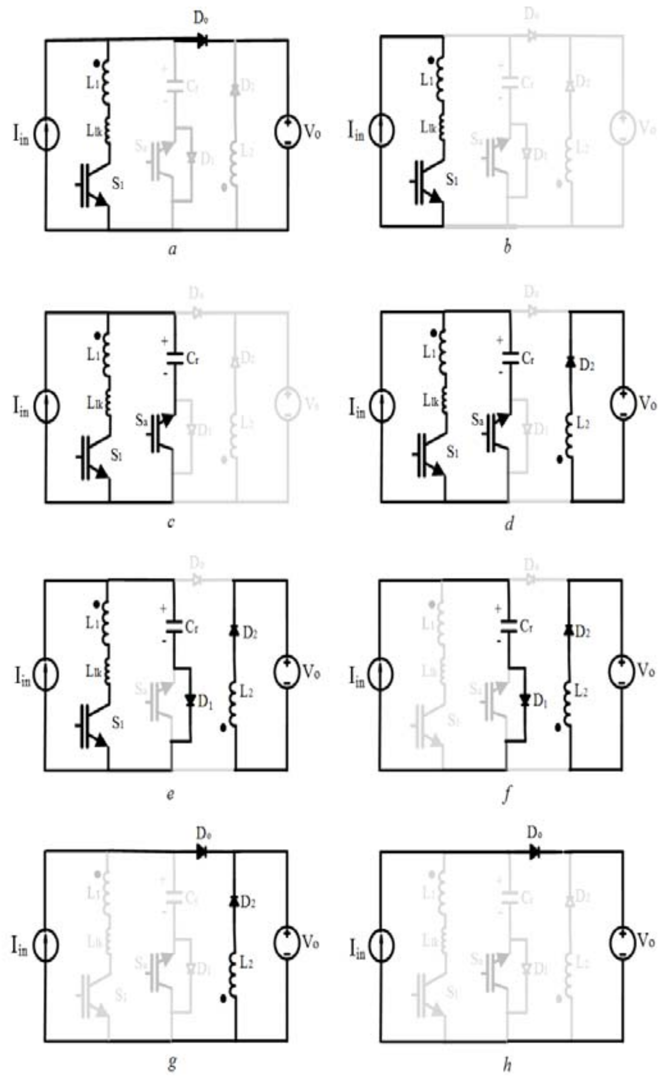

Fig. 2. Equivalent circuit for each operation interval of the proposed boost converter. (a) $[t_0 - t_1]$, (b) $[t_1 - t_2]$, (c) $[t_2 - t_3]$, (d) $[t_3 - t_4]$, (e) $[t_4 - t_5]$, (f) $[t_5 - t_6]$, (g) $[t_6 - t_7]$, (h) $[t_7 - t_8]$.

The theoretical waveforms are illustrated in Fig. 3. Before the first interval, all switches are assumed to be turned off, and I_{in} flows through the main diode D_O to the output; thus, C_r voltage is equal to V_O.

Interval 1: [t_0–t_1] (Fig. 2a): At the beginning of this mode, S_1 is turned on under ZCS condition because of the presence of L_1. According to the following equation, the current of S_1 increases linearly to I_{in}, which prepares the condition for D_O to turn off under ZCS.

$$I_{S1} = \frac{V_O}{L_{lk}+L_1}(t-t_0) \tag{1}$$

At the end of this interval, I_{S1} reaches I_{in}, and D_O is turned off under ZCS.

Interval 2: [t_1–t_2] (*Fig. 2b*): In this mode, I_{in} flows through S_1. This interval is identical to any PWM boost converter when the switch is on.

Interval 3: [t_2–t_3] (*Fig. 2c*): At t_2, S_a is turned on under ZCS, and a resonance among L_1, L_{lk}, and C_r begins through S_1 and S_a. The current and voltage equations are as follows:

$$I_{S1} = I_{in} + \frac{V_O}{Z_1}\sin(\omega_1(t-t_2)) \tag{2}$$

$$V_{C_r} = V_O\cos(\omega_1(t-t_2)) \tag{3}$$

where

$$\omega_1 = \frac{1}{\sqrt{(L_{lk}+L_1)C_r}} \tag{4}$$

$$Z_1 = \sqrt{\frac{L_{lk}+L_1}{C_r}} \tag{5}$$

At the end of this interval, I_{S1} reaches I_1, and C_r discharges to $-V_O/n$.

Interval 4: [t_3–t_4] (*Fig. 2d*): When V_{Cr} reaches $-V_O/n$, D_2 starts to conduct and as a result of the coupling between L_1 and L_2, L_1 voltage is maintained at $-V_O/n$. The resonance between L_{lk} and C_r continues through S_1 and S_a. The voltage and current equations for this interval are given below.

$$I_{S1} = I_{in} + (I_1 - I_{in})\cos(\omega_2(t-t_3)) \tag{6}$$

$$I_{D2} = \frac{1}{n}[(I_{in}-I_1)+(I_1-I_{in})\cos(\omega_2(t-t_3))+\frac{V_O}{nL_1}(t-t_3)] \tag{7}$$

$$V_{C_r} = Z_2(I_{in}-I_1)\sin(\omega_2(t-t_3)) - \frac{V_O}{n} \tag{8}$$

where

$$\omega_2 = \frac{1}{\sqrt{L_{lk}C_r}} \tag{9}$$

$$Z_2 = \sqrt{\frac{L_{lk}}{C_r}} \tag{10}$$

At the end of this interval, I_{S1} decreases to I_{in}, C_r discharges to V_{C1}, and I_{Sa} becomes zero.

$$V_{C1} = Z_2(I_1 - I_{in}) - \frac{V_O}{n} \tag{11}$$

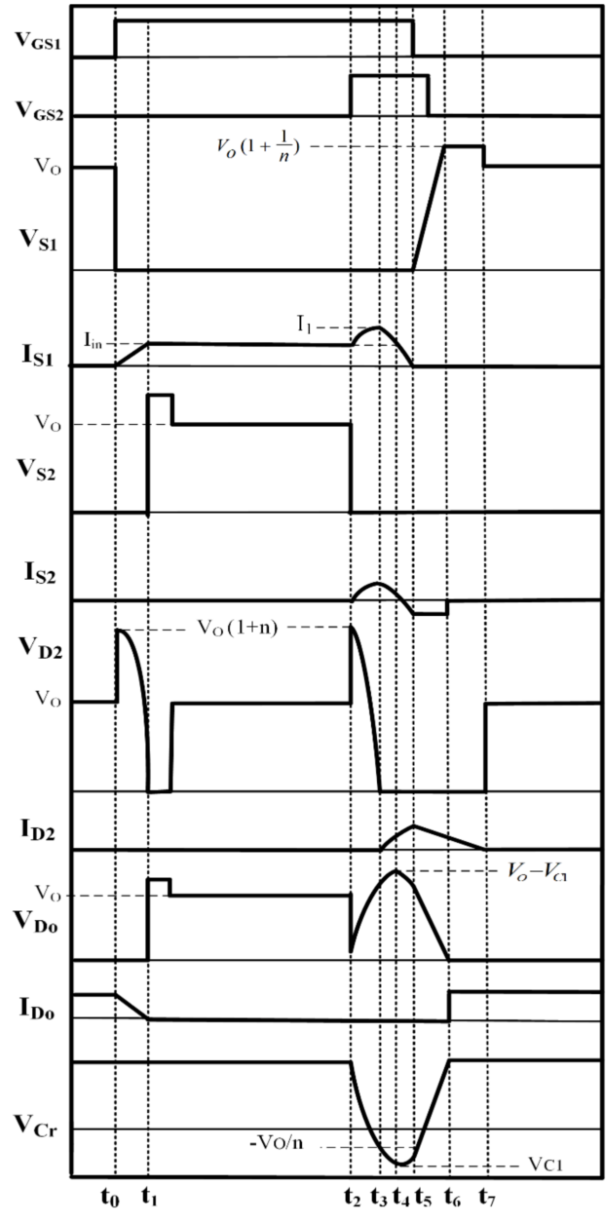

Fig. 3. Key waveforms of the proposed converter.

Interval 5: [t_4–t_5] (*Fig. 2e*): The resonance between L_{lk} and C_r continues through S_1 and the body diode of S_a. Hence, S_a can be turned off under ZCS. In this interval, S_1 and D_2 currents and C_r voltage can be calculated with (6), (7), and (8), respectively. At the end of this interval, I_{S1} becomes zero.

Interval 6: [t_5–t_6] (*Fig. 2f*): At t_5, S_1 current becomes zero and can be turned off under ZCT. As a result of the existence of C_r and based on (14), S_1 voltage rises linearly, which is considered as ZVT. Consequently, S_1 turning off is ZVZCT. The descriptive equations are written as follows:

$$I_{D2} = I_{in} - \frac{V_O}{L_2}(t-t_5) \tag{12}$$

$$V_{C_r} = \frac{I_{in}}{C_r}(t-t_5) - \frac{V_O}{n} \tag{13}$$

$$V_{S1}(t) = \frac{I_{in}}{C_r}(t - t_5) \tag{14}$$

At the end of this interval, C_r voltage reaches V_O. The duration of this mode and the maximum voltage stress of S_1 are

$$\Delta t_6 = t_6 - t_5 = \frac{V_O(n+1)C_r}{nI_{in}} \tag{15}$$

$$V_{S1_{\max}} = V_{S1}(t_6) = V_O(1+\frac{1}{n}) \tag{16}$$

Interval 7: $[t_6–t_7]$ (*Fig. 2g*): At the beginning of this interval, C_r voltage reaches V_O; hence, the body diode of S_a is turned off and D_O can be turned on under ZVS, so I_{in} flows through D_O. When the body diode of S_a is turned off, the voltage of S_a remains zero, and there is a delay between the turn-off instant of the body diode and the voltage rise-up of the auxiliary switch. As a result, S_a is turned off under the ZVZCT condition. In this interval, L_2 current decreases linearly to zero, and D_2 is turned off under ZCS.

Interval 8: $[t_7–t_8]$ (*Fig. 2h*): This operating interval is equal to the turn-off state of regular boost converters, in which I_{in} flows through D_O to the output.

III. Design Procedure

A. Design of Component Values

The input inductor and output capacitor of the converter can be designed as regular PWM converters. L_1 is a snubber inductor that provides ZCS condition for the main switch at turn-on instant. So it can be designed according to [22].

$$L_1 > L_{1,\min} = \frac{V_{sw}.t_r}{I_{sw}} \tag{17}$$

where V_{sw} is the switch voltage before turn-on instant, I_{sw} is the switch current after turn-on, and t_r is the switch current rise time. C_r provides ZCS condition for main switch at turn-off instant. According to (6), the following equation should be satisfied:

$$C_r > C_{r,\min} = \frac{I_{in}^2 L_1}{V_o^2} \tag{18}$$

According to (15), increasing C_r also increases the duration of the sixth interval, the transition time of the main switch at turn-off instant, and, consequently, the conduction losses.

To determine n, the maximum allowable duty cycle should be considered. In this converter, the maximum duty cycle is limited by the discharge time of L_2 in the sixth and seventh intervals. Thus, by using (12), the maximum allowable duty cycle can be calculated as follows:

$$(1 - D_{\max})T_{sw} = \frac{L_2 I_{in}}{V_o} \tag{19}$$

$$D_{\max} = 1 - \frac{n^2 L_1 I_{in} f_{sw}}{V_o} \tag{20}$$

According to (20), a large n results in a decreasing maximum allowable duty cycle and more voltage stress across D_2. However, (16) indicates that larger n leads to lower voltage stress across the main switches. On the basis of (20) and the aforementioned issues, the proper turn ratio (n) can be selected.

B. Power and Frequency Ranges

The proposed converter can be used in various power ranges, as well as other regular ZCT PWM converters and their hard-switching counterparts. In high voltage applications, the voltage stress of D_2, which is equal to $(n+1) V_O$, is increased considerably. However, this limitation is overcome by decreasing n or using series diodes rather than a costly high voltage diode.

In soft-switching PWM converters, the resonant periods must be negligible in comparison with the switching period. The maximum switching frequency can be selected ten times smaller than f_1, but in practice, the switch speed restricts the switching frequency. As a result of the soft-switching condition provided for all semiconductor devices, switching losses become almost zero. Consequently, if the selected resonant frequency is sufficiently high, maximum switching frequency is limited by the operation frequency of the switches, which can be reach a few hundred kHz.

C. Auxiliary Switch Timing

The timing relations between the gate pulse of the main switch and the auxiliary switch are presented in this section. Fig. 4 shows the current and gate pulse waveforms of switches in turn-off instant. According to Fig. 4, before S_1 is turned off, the auxiliary switch is turned on, leading to a resonance between L_1, L_{lk}, and C_r; this resonance provides ZCS condition for the main switch at turn-off instant. The gate pulse of S_1 should be removed when its current becomes zero.

The duration in which the auxiliary switch conducts is shown as α in Fig. 4. According to Figs. 3 and 4 and using (2) and (6), α can be calculated as

$$\alpha \approx \frac{\pi}{2\omega_1} + \frac{\pi}{2\omega_2} \tag{21}$$

β is the time length for decreasing the S_1 current from I_{in} to zero, as shown in Fig. 4. Using (6), β is computed as follows:

$$\beta = \frac{\pi}{2\omega_2} \tag{22}$$

During λ, C_r is charged linearly by I_{in} until its voltage reaches V_O. The duration of λ is Δt_6 according to (15).

To determine the duty cycle of S_a, the maximum and minimum allowable t_{on} of V_{GS2} should be considered. According to Fig. 4, by elapsing α, S_a current reaches zero, then its body diode begins conducting. Therefore, the minimum t_{on} is α.

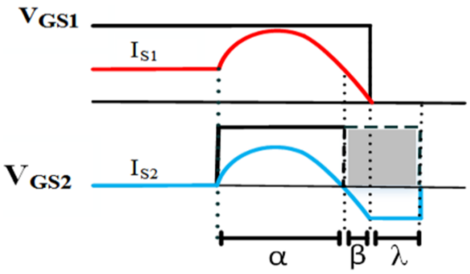

Fig. 4. Waveforms of the current and gate pulse of switches at turn OFF instant.

The body diode of S_a continues to conduct during β and λ; hence, the gate pulse of S_a should be removed during this time. The shaded area in Fig. 4 shows the appropriate time for removing the gate pulse of S_a. Accordingly, on-time of S_a can be calculated as

$$\alpha < t_{ON,Sa} < \alpha + \beta + \lambda \qquad (24)$$

According to Fig. 4, when $\alpha + \beta$ elapses, the current of S_1 becomes zero and it is the proper time for turning off S_1.

IV. Experimental Results

A prototype of the proposed ZCT boost converter is implemented with 50 V input and 100 V output. Table I shows the key parameters of the experimental prototype. A photograph of the implemented prototype is shown in Fig. 5. The experimental waveforms of the main switch, auxiliary switch, and diodes D_2 and D_O shown in Fig. 6–8 confirm the theoretical analysis. Fig. 6 shows that the main switch turns on under ZCS and turns off under simultaneous ZCS and ZVS. To clarify the ZCS condition at turn-on, Fig. 6(b) shows the waveforms of the main switch at turn-on instant.

In the ZCT converters of [23] and [24], the coupled inductors provide soft switching, but the main switch only turns off under ZVS. Consequently, the current of the leakage inductor creates voltage and current spikes at the turn-off instant. In the proposed converter, the main switch turns off under ZCS and ZVS; thus, the current of the leakage inductor discharges completely before turn-off, and perfect ZCZVS is achieved.

Fig. 7(a) illustrates the voltage and current waveforms of the auxiliary switch. Fig. 7(b) indicates that the auxiliary switch turns on under ZCS and turns off under ZCZVS. Fig. 8(a) shows that D_2 turns on with ZVS and ZCS and turns off with ZCS. The voltage stress of D_2 can be lowered by decreasing n, but doing so increases the switch voltage stress.

Fig. 8(b) shows the voltage and current waveforms of the main diode D_O. There is no current stress on D_O, and its voltage stress is less than that of the main diodes in [10], [15] and is less than 2 V_O.

The efficiency curve of the proposed converter and that of ZCT boost converter of [25] are compared using the PSpice software (Fig. 9). The efficiency of the proposed converter is 2.5% greater than that of the ZCT boost of [25] and reaches 97% under full load. The proposed converter achieves a higher efficiency because of the better switching conditions and transfer of circulating energy to the output.

TABLE I

Key Parameters of Experimental Prototype

Parameter	Value
V_{in}	50 V
V_{out}	100 V
P_{out}	100 W
f_{sw}	100 kHz
L_{in}	1 mH
C_o	100 µF
L_1	3 µH
L_2	36 µH
Inductor turns ratio (N_2/N_1)	3
L_{lk}	0.4 µH
C_r	10 nF
Switches	IRG4BC20U
Diodes	BYC15X

Fig. 5. Photograph of the implemented prototype.

The proposed converter and three other ZCT PWM boost converters are compared in Table II. There are fewer extra elements in [8], but its main and auxiliary switches turn on under hard switching, thus decreasing efficiency as power and frequency increase. In [11], circulating energy was reduced and efficiency was improved, but the number of components used was relatively large.

The proposed converter provided better switching conditions than that in [25] for switches and diodes. The current stress of switches and circulating energy decrease considerably because of the coupling effect, which leads to lower losses and higher efficiency. However, the number of the components for the proposed converter is equal to those in [25]; hence, all advantages are achieved without increasing weight or cost. Table III presents the semiconductor losses of the proposed converter with the key parameters mentioned in Table I according to the formula of each component loss [22]. The losses are estimated using component datasheets, whereas the average and RMS values are obtained from the simulation results.

TABLE II
COMPARISON OF ZCT PWM CONVERTERS

	Main switch		Auxiliary switch		Main diode		No. of extra elements
	ON	OFF	ON	OFF	ON	OFF	
Ref. [8]	Hard	ZVZCS	Hard	ZVZCS	ZVS	Hard	4
Ref. [11]	ZCS	ZCS	ZCS	ZCS	ZCS	ZVS	10
Ref. [25]	ZCS	ZCS	ZCS	ZCS	ZCS	ZCS	6
Proposed	ZCS	ZVZCS	ZCS	ZVZCS	ZCS	ZVS	6

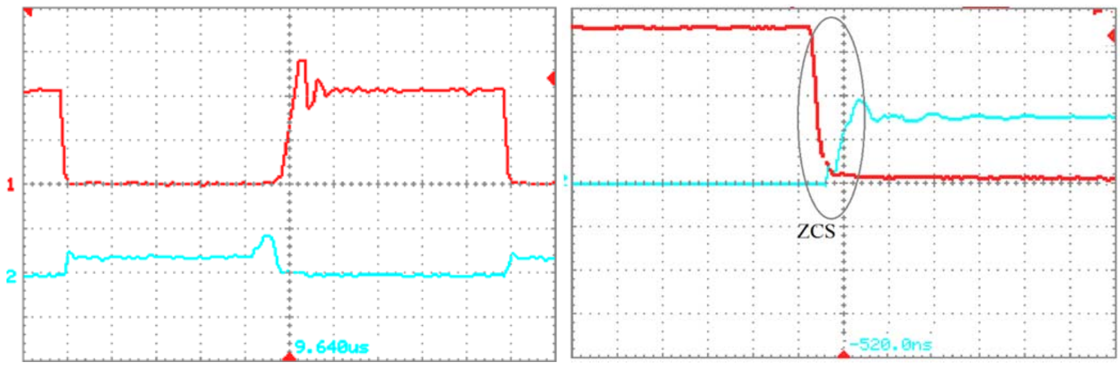

(a) (b)

Fig. 6. Measured voltage (top) and current (bottom) of the main switch S_1. (a) At one switching cycle (vertical axis: 50 V/div or 5 A/div, horizontal axis:1 μs/div). (b) At turn-on instant (vertical axis: 25 V/div or 1.5 A/div, horizontal axis: 250 ns/div).

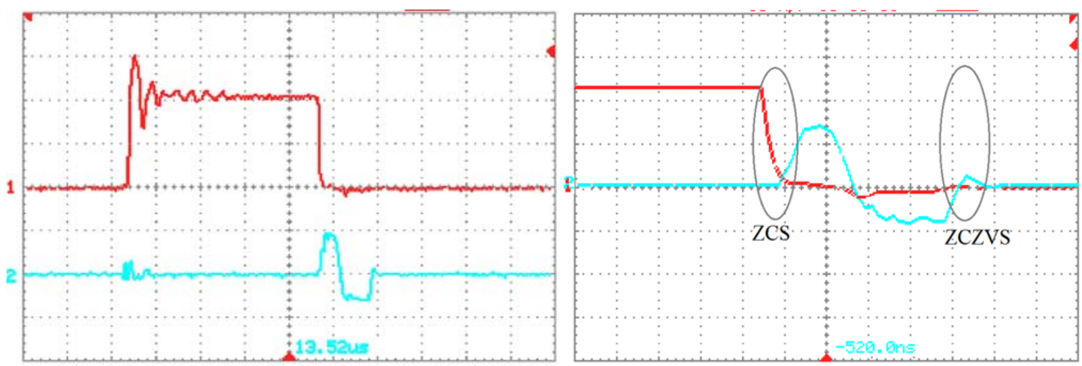

(a) (b)

Fig. 7. Measured voltage (top) and current (bottom) of the auxiliary switch S_a. (a) At one switching cycle (vertical axis: 50 V/div or 3 A/div, horizontal axis:1 μs/div). (b) At turn-on instant (vertical axis: 50 V/div or 2 A/div, horizontal axis: 250 ns/div).

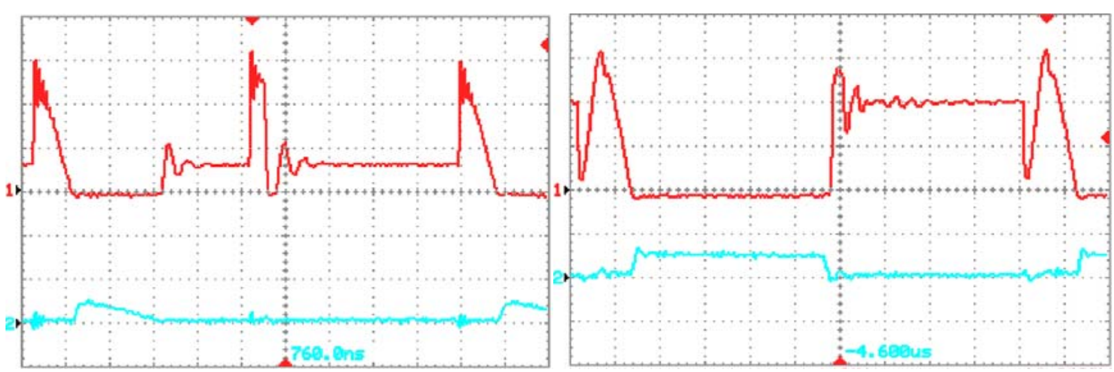

(a) (b)

Fig. 8. Measured voltage (top) and current (bottom) of (a) diode D_2 (vertical axis: 150 V/div or 5 A/div, horizontal axis: 1 μs/div) and (b) main diode (vertical axis: 50 V/div or 5A/div, horizontal axis: 1 μs/div).

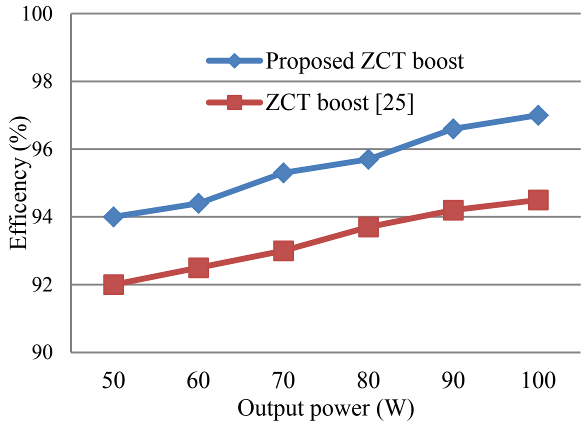

Fig. 9. Efficiency of ZCT boost converters (proposed and [25]).

TABLE III
SEMICONDUCTOR LOSSES IN PROPOSED ZCT BOOST CONVERTER

Type of loss	Value (W)
S_1 and S_a switching loss **$\frac{1}{2}.V_O.I_{in}(t_{on} + t_{off}).f_{sw}$**	Zero due to soft switching
S_1 conduction loss **$I_{ave,S1}.V_{CE(on)}$**	1.8
S_a conduction loss **$I_{ave,Sa}.V_{CE(on)}$**	135×10^{-3}
Parasitic capacitance loss in S_1 **$1/2.C_{out}.V_O^2.f_{sw}$**	25×10^{-3}
Parasitic capacitance loss in S_a **$1/2.C_{out}.V_O^2.f_{sw}$**	25×10^{-3}
D_O conduction loss **$V_F . I_{ave,Do}$**	0.9
D_1 conduction loss **$V_F . I_{ave,D1}$**	112×10^{-3}
D_2 conduction loss **$V_F . I_{ave,D2}$**	68×10^{-3}
S_1 gate drive loss **$Q_q.V_{GE}.f_{sw}$**	39×10^{-3}
S_a gate drive loss **$Q_q.V_{GE}.f_{sw}$**	39×10^{-3}
Total loss	3.14 W

V. CONDUCTED EMI MEASUREMENT

This section presents the experimental results of the conducted EMI measurement for the proposed converters and ZCT boost [25]. A line impedance stabilization network (LISN) according to CISPR22 standard is used to measure conducted electromagnetic emissions [26]. The conducted EMI spectrums are measured using a GW-INSTEK spectrum analyzer (peak detection mode) (as shown in Fig. 10 and Fig. 11 for 150 kHz- 30 MHz.

Figs. 10 and 11 show that the main EMI peaks of the proposed and ZCT converters [25] are approximately 82 dBµV at 7 MHz and 90 dBµV at 9.7 MHz, respectively. Consequently, the main EMI peak of the proposed converter is 8 dBµV lower than the main EMI peak of [25] because of the soft switching conditions provided for all semiconductor devices. The conducted electromagnetic emissions of the proposed and ZCT boost converters [25] are compared in Fig. 12 under various frequency ranges. The effect of the

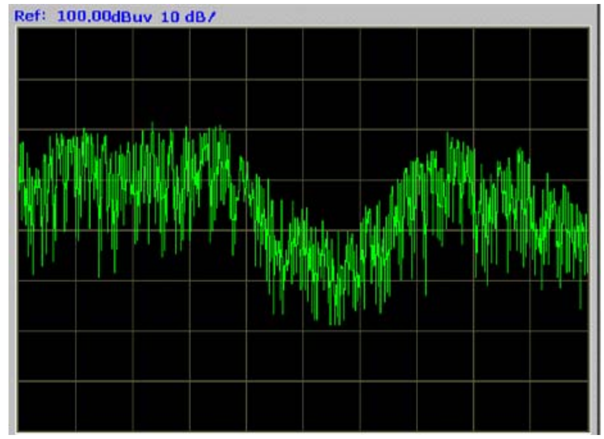

Fig. 10. Conducted EMI measurement of proposed ZCT boost converter (vertical axis: 20–100 dBµV, horizontal axis: 0.15–30 MHz).

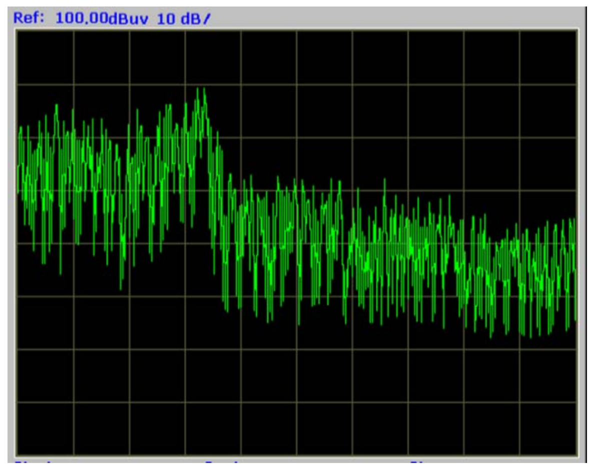

Fig. 11. Conducted EMI measurement of ZCT boost converter in [25] (vertical axis: 20–100 dBµV, horizontal axis: 0.15–30 MHz).

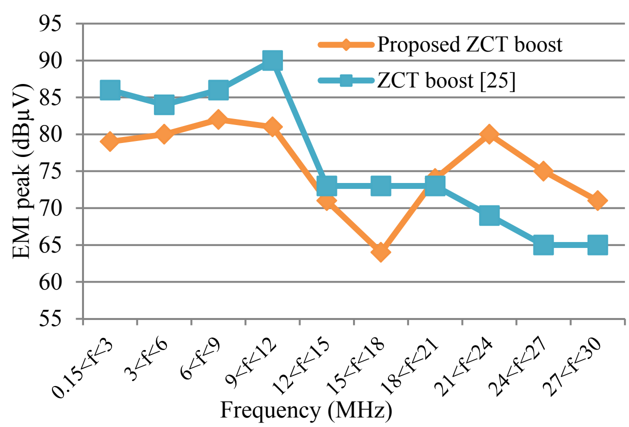

Fig. 12. Comparison of conducted EMI peaks in various frequency ranges (experimental results).

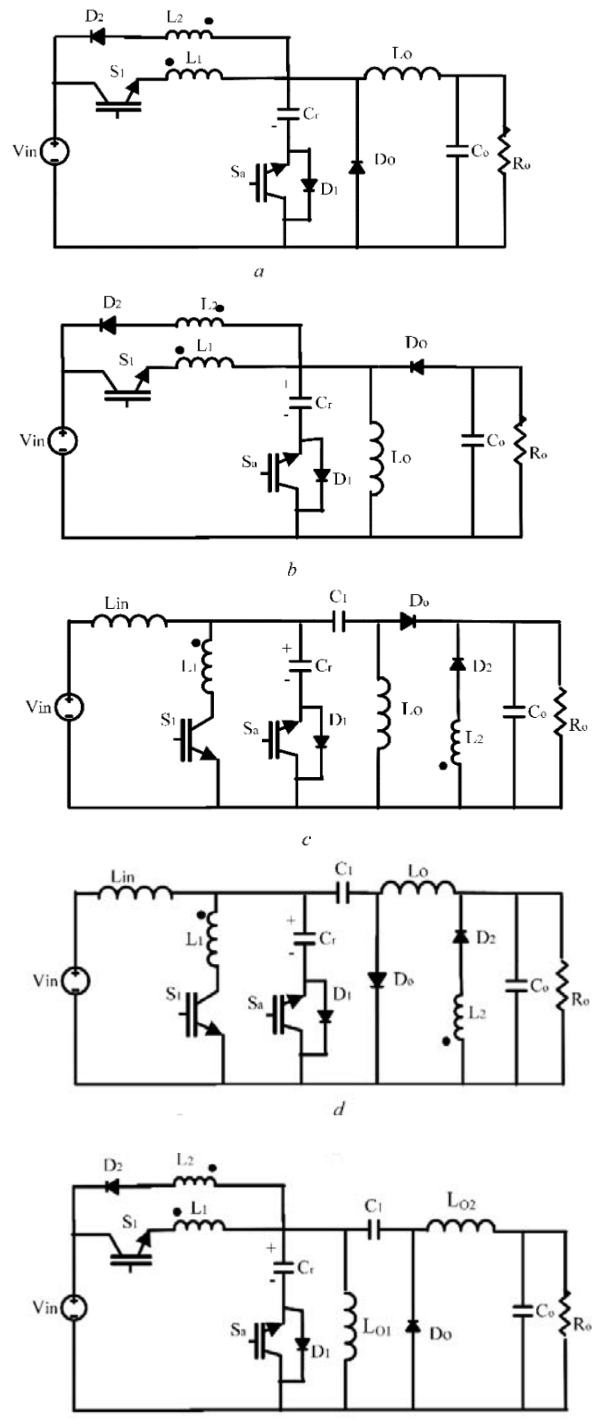

Fig. 13. Proposed family of ZCT PWM converters: (a) buck, (b) buck-boost, (c) Cuk, (d) SEPIC, and (e) zeta.

proposed ZCT–ZVT method on EMI reduction is significant at frequencies up to 21 MHz. Although the proposed and mentioned converters provide ZCS that leads to lower *di/dt*, the proposed converter provides ZVS, which also reduces *dv/dt*. Thus, the proposed boost converter achieves better performance in terms of EMC because of the lower main EMI peak.

VI. Other ZCT PWM Converters

The proposed ZCT method can be applied to other basic PWM converters, such as buck, buck-boost, Cuk, SEPIC, and zeta converters (Fig. 13). In these topologies, the operation intervals are similar to those of the boost converter in Section II.

VII. Conclusion

A new family of ZCT PWM converters is introduced. All semiconductor devices in the proposed converters operate under soft-switching conditions. On the basis of this family, the boost topology is selected. The analysis of the interval modes shows that the main switch turns on with ZCS and turns off with ZCT and ZVT. Moreover, the auxiliary switch turns on under ZCT and turns off under ZVZCT. The additional benefits of the proposed converters included low circulating energy and current stress. A ZCT boost converter from the proposed family is designed and implemented with the proposed design procedure. The experimental results of the prototype confirm the theoretical analysis. That is, the proposed converter achieves a higher efficiency and lower conducted emissions in comparison with another ZCT boost converter.

References

[1] C. M. Wang, C. H. Lin, and C. H. Cheng, "Analysis, design and realization of a zero-current transition pulse-width modulation interleaved boost power factor correction converter with a zero-current transition auxiliary circuit," *IET Power Electronics*, Vol. 8, No. 9, pp. 1777-1785, Sep. 2015.

[2] Q. Lou, Y. Zhang, P. Sun, and L. Zhou, "An active clamp high step-up boost converter with a coupled inductor," *Journal of Power Electronics*, Vol. 15, No. 1, pp. 86- 95, Jan. 2015.

[3] X. Wei, C. Lou, H. Nan, and Y. Wang, "A simple structure of zero-voltage switching (ZVS) and zero-current switching (ZCS) buck converter with coupled inductor," *Journal of Power Electronics*, Vol. 15, No. 6, pp. 1480-1488, Nov. 2015.

[4] L. S. Yang and C. C. Lin, "Analysis and implementation of a DC-DC converter for hybrid power supplies systems," *Journal of Power Electronics*, Vol. 15, No. 6, pp. 1438-1445, Nov. 2015.

[5] H. F. Xiao, K. Lan, B. Zhou, L. Zhang, and Z. Wu, "A family of zero-current-transition transformerless photovoltaic grid-connected inverter," *IEEE Trans. Power Electron.*, Vol. 30, No. 6, pp. 3156-3165, Jun. 2015.

[6] J. H. Kim, D. Y. Jung, S. H. Park, C. Y. Won, Y. C. Jung, and S. W. Lee, "High efficiency soft-switching boost converter using a single switch," *Journal of Power Electronics*, Vol. 9, No. 6, pp. 929-939, Nov. 2009.

[7] K. S. Bin Muhammad and D. D.–C. Lu, "ZCS bridgeless boost PFC rectifier using only two active switches," *IEEE Trans. Ind. Electron.*, Vol. 62, No. 5, pp. 2795-2806, May 2015.

[8] C. E. Kim, E. S. Park, and G. W. Moon, "New

zero-current-transition (ZCT) circuit cell without additional current stress," *Journal of Power Electronics*, Vol. 3, No. 4, pp. 215- 223, Oct. 2003.
[9] M. Jabbari, S. Sharifi, and G. Shahgholian, "Resonant CLL non-inverting buck-boost converter," *Journal of Power Electronics*, Vol. 13, No. 1, pp. 1-8, Jan. 2013.
[10] H. S. Park and B. H. Cho, "Improved zero-current-switching (ZCS) PWM switch cell with minimum additional conduction losses," *Journal of Power Electronics*, Vol. 1, No. 2, pp. 71-77, Mar. 2001.
[11] P. Das and G. Moschopoulos, "A comparative study of zero-current-transition PWM converters," *IEEE Trans. Ind. Electron.*, Vol. 54, No. 3, pp. 1319-1328, Jun. 2007.
[12] H. Mao, F. C. Y. Lee, X. Zhou, H. Dai, M. Cosan, and D. Boroyevich, "Improved zero-current-transition converters for high-power applications," *IEEE Trans. Ind. Appl.*, Vol. 33, No. 5, pp. 1220 -1232, Sep./Oct. 1997.
[13] E. Adib and H. Farzanehfard, "Family of isolated zero current transition PWM converters," *Journal of Power Electronics*, Vol. 9, No. 2, pp. 156-163, Mar. 2009.
[14] M. Jabbari, H. Farzanehfard, and G. Shahgholian, "Isolated topologies of switched-resonator converters," *Journal of Power Electronics*, Vol. 10, No. 2, pp. 125- 131, Mar. 2010.
[15] E. Adib and H. Farzanehfard, "Family of zero current transition PWM converters," *IEEE Trans. Ind. Electron.*, Vol. 55, No. 8, pp. 3055- 3063, Aug. 2008.
[16] H. S. Kim, J. W. Baek, M. H. Ryu, J. H. Kim, and J. H. Jung, "Passive lossless snubbers using the coupled inductor method for the soft switching capability of boost PFC rectifiers," *Journal of Power Electronics*, Vol. 15, No. 2, pp. 366- 377, Mar. 2015.
[17] S. J. Kim and H. L. Do, "Soft-switching step-up converter with ripple-free output current," *IEEE Trans. Power. Electron.*, Vol. 31, No. 8, pp. 5618- 5624, Aug. 2016.
[18] M. Mohammadi, E. Adib, and M. R. Yazdani, "Family of soft-switching single-switch PWM converters with lossless passive snubber," *IEEE Trans. Ind. Electron*., Vol. 62, No. 6, pp. 3473- 3481, Jun. 2015.
[19] M. R. Yazdani, S. Rahmani, and M. Mohammadi, "A ZCT double-ended flyback converter with low EMI," *Journal of Power Electronics*, Vol. 15, No. 3, pp. 602- 609, May 2015.
[20] M. R. Yazdani, H. Farzanehfard, and J. Faiz, "Classification and comparison of EMI mitigation techniques in switching power converters – a review," *Journal of Power Electronics*, Vol. 11, No. 5, pp.767-777, Sep. 2011.
[21] M. R. Yazdani, H. Farzanehfard, and J. Faiz, "EMI analysis and evaluation of an improved ZCT flyback converter," *IEEE Trans. Power Electron.*, Vol. 26, No. 8, pp. 2326- 2334, Aug. 2011.
[22] N. Mohan, T. M. Undeland, and W. P. Robbins, *Power Electronics*, Wiley, 3rd edition, 2003.
[23] M. R. Amini and H. Farzanehfard, "Novel family of PWM soft-single-switched dc-dc converters with coupled inductors," *IEEE Trans. Ind. Electron.*, Vol. 56, No. 6, pp. 2108- 2114, Jun. 2009.
[24] E. Adib and H. Farzanehfard, "Family of soft-switching PWM converters with current sharing in switches," *IEEE Trans. Power Electron.*, Vol. 24, No. 4, pp. 979- 984, Apr. 2009.
[25] M. Ahmadi, M. R. Mohammadi, E. Adib, and H. Farzanehfard, "Family of non-isolated zero current transition bi-directional converters with one auxiliary switch," *IET Power Electronics*, Vol. 5, No. 2, pp. 158-165, Feb. 2012.
[26] IEC International Special Committee on Radio Interference – C.I.S.P.R., "Information Technology Equipment-Radio Disturbance Characteristics-Limits and Methods of Measurement," *International Electrotechnical Commission*, Publication 22, 1997.

Mohammad Rouhollah Yazdani was born in Isfahan, Iran, in 1978. He received his B.S., M.S., and Ph.D. degrees in Electrical Engineering from the Isfahan University of Technology, Najafabad Branch in 2001; Islamic Azad University in 2004; and Sciences & Research Branch, Islamic Azad University in 2011, respectively. Since 2011, he has been a Faculty Member at the Department of Electrical and Computer Engineering, Isfahan (Khorasgan) Branch, Islamic Azad University, Isfahan, Iran. His research interests include soft-switching converters, EMI reduction techniques, signal integrity, and EMC issues.

Mohammad Pahlavan Dust was born in Kashan, Iran, in 1991. He received his B. S. degree in Electrical Engineering from Isfahan (Khorasgan) Branch, Islamic Azad University, Isfahan, Iran, and he is currently working toward his M.S. degree in Electrical Engineering. Since 2013, he has been a member of the young researchers and elite club of the Islamic Azad University. His current research interests include soft-switching power converters and EMI.

Poorya Hemmati was born in Isfahan, Iran, in 1992. He received his B.S. degree in Electrical Engineering from Isfahan (Khorasgan) Branch, Islamic Azad University, Isfahan, Iran. Since 2014, he has worked in the electrical research center of the Isfahan (Khorasgan) Branch, Islamic Azad University, where he is also serving as a Lab Assistant. His main research interests are renewable energies and switching power supplies.